INTERNATIONAL JOURNAL FOR NUMERICAL METHODS IN FLUIDS
Int. J. Numer. Meth. Fluids 2008; **58**:727–741
Published online 18 February 2008 in Wiley InterScience (www.interscience.wiley.com). DOI: 10.1002/fld.1760

Numerical simulations of viscous flows using a meshless method

Changfu You[1,*,†], Yi Qiu[1], Xuchang Xu[1] and Delong Xu[2]

[1]*Key Laboratory for Thermal Science and Power Engineering of Ministry of Education, Department of Thermal Engineering, Tsinghua University, Beijing 100084, China*
[2]*Xi'an University of Architecture & Technology, Xi'an, Shanxi, China*

SUMMARY

This paper uses the element-free Galerkin (EFG) method to simulate 2D, viscous, incompressible flows. The control equations are discretized with the standard Galerkin method in space and a fractional step finite element scheme in time. Regular background cells are used for the quadrature. Several classical fluid mechanics problems were analyzed including flow in a pipe, flow past a step and flow in a driven cavity. The flow field computed with the EFG method compared well with those calculated using the finite element method (FEM) and finite difference method. The simulations show that although EFG is more expensive computationally than FEM, it is capable of dealing with cases where the nodes are poorly distributed or even overlap with each other; hence, it may be used to resolve remeshing problems in direct numerical simulations. Flows around a cylinder for different Reynolds numbers are also simulated to study the flow patterns for various conditions and the drag and lift forces exerted by the fluid on the cylinder. These forces are calculated by integrating the pressure and shear forces over the cylinder surface. The results show how the drag and lift forces oscillate for high Reynolds numbers. The calculated Strouhal number agrees well with previous results. Copyright © 2008 John Wiley & Sons, Ltd.

Received 19 October 2006; Revised 20 October 2007; Accepted 7 December 2007

KEY WORDS: viscous incompressible flows; meshless method; EFG; fractional step method; numerical simulation

1. BACKGROUND

Meshless methods originated about 20 years ago with several branches such as smoothed particle hydrodynamics [1], reproducing kernel particle method [2], diffuse element method [3] and element-free Galerkin method (EFG) [4]. The objective of meshless methods is to eliminate at least part of the mesh by constructing an approximation entirely in terms of nodes.

*Correspondence to: Changfu You, Key Laboratory for Thermal Science and Power Engineering of Ministry of Education, Department of Thermal Engineering, Tsinghua University, Beijing 100084, China.
†E-mail: youcf@tsinghua.edu.cn

Contract/grant sponsor: National Natural Science Foundation of China; contract/grant number: 50432040
Contract/grant sponsor: Special Funds for Major State Basic Research Projects; contract/grant number: 2006CB200305

At present, meshless methods are mainly applied in the field of solid mechanics, which have some advantages for simulations of molding and crack propagation [4, 5]. There have been few applications of meshless methods in fluid mechanics, since finite element method (FEM) and finite difference method (FDM) are able to solve most fluid problems. However, for some particular cases such as interface/free-face flows [6] and fluid–particle flows, methods based on meshes such as the FEM have to remesh at each step as the flow evolves so that the mesh lines remain coincident with the moving surfaces or boundaries throughout the solution. This introduces numerous difficulties such as the need to project between meshes in successive stages of the problem, which leads to degradation of accuracy and complexity in the computer program, not to mention the burden associated with a large number of remeshings [7]. Although many meshless methods require meshes in at least part of the domain, moving boundaries can usually be treated without remeshing with minor costs in accuracy degradation. Thus, large classes of problems can be solved, which are very awkward with mesh-based methods.

We use this method in fluid dynamics in order to solve these kinds of problems such as the particle collision problem in multiphase flows. The restriction of meshes makes it very difficult for mesh-based direct numerical simulation methods to deal with cases where there are particle collisions. Hence, the particle collision becomes a key problem in the direct numerical simulation of in multiphase flows. Daniel D. Joseph said [8], 'It is not possible to simulate the motion of even a moderately dense suspension of particles without a strategy to handle cases in which particles touch.' First of all, we use some classic examples to prove the accuracy and precision of this method. In this paper, the EFG method was used to simulate 2D, viscous, incompressible flows. The results from the EFG method are compared with FEM and FDM predictions. The advantages and disadvantages of the applications of EFG and FEM in fluid mechanics are discussed as well. Furthermore, the unsteady flow around a 2D cylinder is also analyzed to predict the flow patterns for different Reynolds numbers. The predicted Strouhal number for vortex shedding is in good agreement with previous results. Our further research is to realize real collisions between particles with this meshless method.

2. THE EFG METHOD

Consider an approximation of a single function $u(x)$ in a domain Ω. The domain Ω is assumed to be described by the usual methods of computational geometry. Within the domain, a set of nodes x_I, $I=1$ to n, is constructed and the approximation associated with the function at node I is denoted by u_I.

A common feature of all meshless methods is a weight function. A weight function is defined to have compact support, i.e. the subdomain over which it is nonzero is small relative to the rest of the domain. Each subdomain Ω_I is associated with a node I. The support is often called the domain of influence of a node. The most commonly used subdomains are discs or rectangles, as shown in Figure 1. The domain here is indicated by bold lines with thin lines used for the supports of the weight function.

The EFG method uses the moving least-square approximation to construct the shape functions. In the approximation, let

$$u(\mathbf{x})=\sum_{j=1}^{m} p_j(\mathbf{x})a_j(\mathbf{x})=\mathbf{p}^{\mathrm{T}}(\mathbf{x})\mathbf{a}(\mathbf{x}) \tag{1}$$

DOI: 10.1002/fld

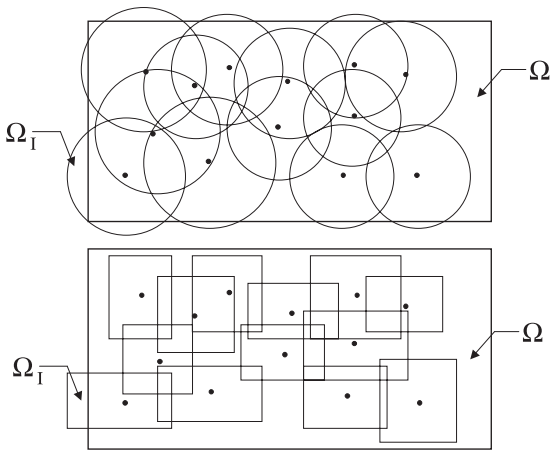

Figure 1. Computational model for a meshless method showing the boundary, nodes and supports.

where m is the number of terms in the basis function, $p_i(x)$ are monomial basis functions and $a_i(x)$ are their coefficients, which are functions of the spatial coordinate x. The commonly used 2D basis is the linear basis

$$\mathbf{p}^{\mathrm{T}}(\mathbf{x}) = [1 \;\; x \;\; y], \quad m = 3$$

Lancaster and Salkauskas [9] defined a local approximation by

$$u^h(\mathbf{x}, \overline{\mathbf{x}}) = \sum_{j=1}^{m} p_j(\overline{\mathbf{x}}) a_j(\mathbf{x}) = \mathbf{p}^{\mathrm{T}}(\overline{\mathbf{x}})\mathbf{a}(\mathbf{x}) \tag{2}$$

$\overline{\mathbf{x}}$ is the spatial coordinate of nodes that are in the domain of point x. The coefficients $a_i(x)$ are obtained by performing a weighted least-square fit for the local approximation, which is obtained by minimizing the difference between the local approximation and the function. This yields the quadratic form

$$J(\mathbf{x}) = \sum_{I=1}^{n} w(\mathbf{x}-\mathbf{x}_I)[u(\mathbf{x}, \mathbf{x}_I) - u_I]^2 = \sum_{I=1}^{n} w(\mathbf{x}-\mathbf{x}_I)[\mathbf{p}^{\mathrm{T}}(\mathbf{x}_I)\mathbf{a}(\mathbf{x}) - u_I]^2 \tag{3}$$

where $w(\mathbf{x}-\mathbf{x}_I)$ is a weighting function with compact support and n is the number of the nodes that have an effect on point x. The least-square method is used to find the coefficients $a(x)$

$$\frac{\partial J(\mathbf{x})}{\partial \mathbf{a}(\mathbf{x})} = \mathbf{A}(\mathbf{x})\mathbf{a}(\mathbf{x}) - \mathbf{B}(\mathbf{x})\mathbf{u} = 0 \tag{4}$$

where $\mathbf{A}(\mathbf{x}) = \mathbf{P}^{\mathrm{T}}\mathbf{W}(\mathbf{x})\mathbf{P}$ and $\mathbf{B}(\mathbf{x}) = \mathbf{P}^{\mathrm{T}}\mathbf{W}(\mathbf{x})$, then

$$\mathbf{a}(\mathbf{x}) = \mathbf{A}^{-1}(\mathbf{x})\mathbf{B}(\mathbf{x})\mathbf{u} \tag{5}$$

Substituting Equation (5) into Equation (1) gives

$$\mathbf{u}(\mathbf{x}) = \mathbf{P}^{\mathrm{T}}(\mathbf{x})\mathbf{A}^{-1}(\mathbf{x})\mathbf{B}(\mathbf{x})\mathbf{u} \tag{6}$$

DOI: 10.1002/fld

The weight function greatly influences the methodology. In this paper [10]

$$w_I(\mathbf{x})=\begin{cases}\dfrac{r_i^2}{r_I^2+1}\left(1-\dfrac{r_i^2}{r_I^2}\right)^8, & r_I\leqslant r_i\\ 0, & r_I>r_i\end{cases} \tag{7}$$

where $r_I=\|\mathbf{x}-\mathbf{x}_I\|$ is the distance from $\mathbf{x}$ to $\mathbf{x}_I$, and r_i is the radius of the influence domain of node I.

3. CONTROL EQUATIONS AND DISCRETIZATION

The control equations for 2D, viscous, incompressible flow are

$$\begin{aligned}\frac{\partial u_i}{\partial t}+u_j u_{i,j}&=-\frac{p_{,i}}{\rho}+\nu(u_{i,j}+u_{j,i})_{,j}+f_i\\ u_{i,i}&=0\end{aligned} \tag{8}$$

Using the three-step finite element scheme introduced by Jiang *et al.* [11]

$$\begin{aligned}\frac{u_i^{n+1/3}-u_i^n}{\Delta t/3}&=-u_j^n u_{i,j}^n-\frac{p_{,i}^n}{\rho}+\nu(u_{i,j}^n+u_{j,i}^n)_{,j}+f_i^n\\ \frac{u_i^{n+1/2}-u_i^n}{\Delta t/2}&=-u_j^{n+1/3}u_{i,j}^{n+1/3}-\frac{p_{,i}^n}{\rho}+\nu(u_{i,j}^{n+1/3}+u_{j,i}^{n+1/3})_{,j}+f_i^{n+1/3}\\ \frac{u_i^{n+1}-u_i^n}{\Delta t}&=-u_j^{n+1/2}u_{i,j}^{n+1/2}-\frac{p_{,i}^{n+1}}{\rho}+\nu(u_{i,j}^{n+1/2}+u_{j,i}^{n+1/2})_{,j}+f_i^{n+1/2}\end{aligned} \tag{9}$$

Then discretizing Equation (9) with the standard Galerkin method,

$$\begin{aligned}M_{\alpha\beta}\frac{u_{i\beta}^{n+1/3}-u_{i\beta}^n}{\Delta t/3}&=-N_{\alpha\beta}^n u_{i\beta}^n-\frac{L_{i\alpha\beta}p_\beta^n}{\rho}-\nu S_{i\alpha}^n+M_{\alpha\beta}f_{i\beta}^n\\ &\quad+\int_\Gamma \Phi_\alpha \nu(u_{i,j}^n+u_{j,i}^n)\cdot n_i\,\mathrm{d}\Gamma\end{aligned} \tag{10}$$

$$\begin{aligned}M_{\alpha\beta}\frac{u_{i\beta}^{n+1/2}-u_{i\beta}^{n+1/3}}{\Delta t/2}&=-N_{\alpha\beta}^{n+1/3}u_{i\beta}^{n+1/3}-\frac{L_{i\alpha\beta}p_\beta^n}{\rho}-\nu S_{i\alpha}^{n+1/3}+M_{\alpha\beta}f_{i\beta}^{n+1/3}\\ &\quad+\int_\Gamma \Phi_\alpha \nu(u_{i,j}^{n+1/3}+u_{j,i}^{n+1/3})\cdot n_i\,\mathrm{d}\Gamma\end{aligned}$$

DOI: 10.1002/fld

$$M_{\alpha\beta}\frac{u_{i\beta}^{n}-u_{i\beta}^{n+1/2}}{\Delta t}=-N_{\alpha\beta}^{n+1/2}u_{i\beta}^{n+1/2}-\frac{L_{i\alpha\beta}p_{\beta}^{n+1}}{\rho}-\nu S_{i\alpha}^{n+1/2}+M_{\alpha\beta}f_{i\beta}^{n+1/2}$$
$$+\int_{\Gamma}\Phi_{\alpha}\nu(u_{i,j}^{n+1/2}+u_{j,i}^{n+1/2})\cdot n_i\,\mathrm{d}\Gamma$$

where the subscript β indicates summation over all values of β and

$$\begin{aligned}M_{\alpha\beta}&=\int\int_{\Omega^e}\Phi_{\alpha}\Phi_{\beta}\,\mathrm{d}\Omega\\ L_{i\alpha\beta}&=\int\int_{\Omega^e}\Phi_{\alpha}\Phi_{\beta,i}\,\mathrm{d}\Omega\\ N_{\alpha\beta}^{n}&=\int\int_{\Omega^e}\Phi_{\alpha}\Phi_{\nu}\Phi_{\beta,j}u_{j\nu}^{n}\,\mathrm{d}\Omega\\ S_{i\alpha}^{n}&=\int\int_{\Omega}\Phi_{\alpha,i}(\Phi_{\beta,j}u_{i\beta}^{n}+\Phi_{\beta,i}u_{j\beta}^{n})\,\mathrm{d}\Omega\end{aligned}\tag{11}$$

As Equation (10) shows, u_i^{n+1} can only be calculated after p^{n+1} is calculated. The last formula in Equation (10) gives the pressure Poisson equation for EFG

$$\frac{G_{\alpha\beta}p_{\beta}^{n+1}}{\rho}=-\frac{1}{\Delta t}H_{i\alpha\beta}u_{i\beta}^{n}-K_{j\alpha\beta}u_{j\beta}^{n+1/2}-S_{\alpha}\tag{12}$$

where

$$\begin{aligned}G_{\alpha\beta}&=\int\int_{\Omega^e}\Phi_{\alpha,i}\Phi_{\beta,i}\,\mathrm{d}\Omega\\ H_{i\alpha\beta}&=\int\int_{\Omega^e}\Phi_{\alpha}\Phi_{\beta,i}\,\mathrm{d}\Omega\\ K_{j\alpha\beta}&=\int\int_{\Omega^e}\Phi_{\alpha,i}\Phi_{\beta}\Phi_{\nu,j}u_{i\nu}^{n+1/2}\,\mathrm{d}\Omega\\ S_{\alpha}&=\int_{\Gamma}\Phi_{\alpha}\frac{u_i^{n+1}-u_i^{n}}{\Delta t}\,\mathrm{d}\Gamma\end{aligned}\tag{13}$$

After p^{n+1} is obtained from Equation (12), u_i^{n+1} is calculated using Equation (10). This three-step finite element scheme, which has no artificial parameters, is stable, even for high Reynolds number simulations.

The approximate function of EFG is not determined by node variables. That is to say,

$$\phi_I(\mathbf{x}_J)\neq\delta_{IJ},\quad\begin{cases}\delta_{IJ}=1, & I=J\\ \delta_{IJ}=0, & I\neq J\end{cases}$$

Compared with FEM, it is more difficult to use boundary conditions. We use the Lagrange multiplier method [12] to deal with boundary conditions.

DOI: 10.1002/fld

4. RESULTS AND DISCUSSIONS

Several classical 2D problems were solved here using the EFG method with the results than compared with those from FEM and FDM calculations. There are time domains and in the initial time, zero is assigned to the initial values of parameters at the nodes. The time step is $0.5e-01$ s in all cases. The robustness of EFG is better than the FEM and FDM, and the irregular distribution has little effect on the calculation results, as the FEM and FDM are not suitable for the irregular distribution [13]. In order to compare with the FEM and FDM, the nodes are regularly distribution.

Case 1: *Flow in a pipe*. The pipe was 1 m long and 0.5 m wide. The fluid parameters were $\rho = 1.21\,\mathrm{kg/m^3}$, $\gamma = 14.9 \times 10^{-6}\,\mathrm{m^2/s}$ and an inlet velocity of $V = 1.0\,\mathrm{mm/s}$. The simulation used $101 * 51$ nodes regularly distributed in the computational domain. The FEM used triangular elements that connected these nodes, but the EFG method did not generate elements.

The x direction velocities at $x = 0.5\,\mathrm{m}$ computed by FDM, FEM and EFG are given in Figure 2. This figure shows that the EFG results agree well with those of FDM and FEM, as the curves almost overlap each other.

Case 2: *Flow past a step*. The computational domain is shown in Figure 3. The fluid parameters were $\rho = 1.21\,\mathrm{kg/m^3}$, $\gamma = 14.9 \times 10^{-6}\,\mathrm{m^2/s}$ and an inlet velocity of $V = 1.0\,\mathrm{mm/s}$. 10 301 nodes were regularly distributed in the domain. Figure 3 shows the velocity field for the vortex behind the step. The x direction velocities at $x = 2.5\,\mathrm{m}$ are compared in Figure 4 with little difference between the FDM, FEM and EFG results as shown in Figure 4.

Case 3: *Flow in a driven cavity*. The domain was $0.5\,\mathrm{m} * 0.5\,\mathrm{m}$. The fluid parameters were $\rho = 1.21\,\mathrm{kg/m^3}$, $\gamma = 14.9 \times 10^{-6}\,\mathrm{m^2/s}$, and a Reynolds number of 400. $51 * 51$ nodes were regularly distributed in the domain.

The x direction velocities at $x = 0.25\,\mathrm{m}$ are compared in Figure 5. The EFG results agree well with the FEM results, while there was some difference with FDM results.

In the simulations, the EFG calculations required more time than the FEM calculations, which is the main disadvantage of the EFG method. However, for the FEM, once the mesh nodes in

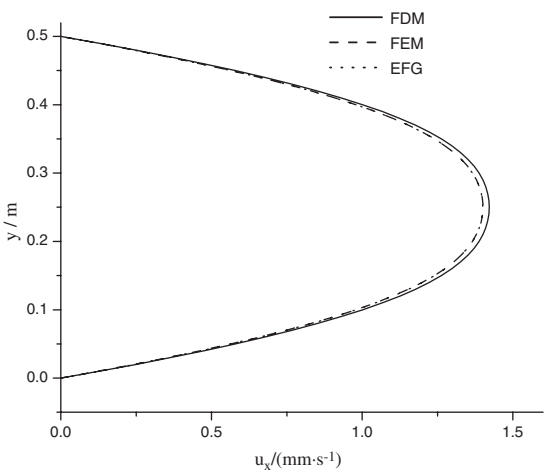

Figure 2. u_x distribution at $X = 0.5\,\mathrm{m}$ for flow in a pipe for $Re = 33.6$.

DOI: 10.1002/fld

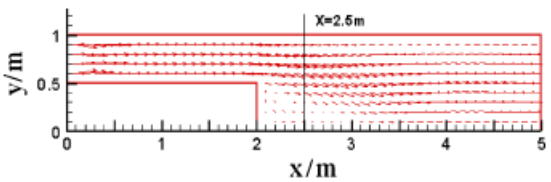

Figure 3. Velocity field for flow past a step for $Re = 33.6$.

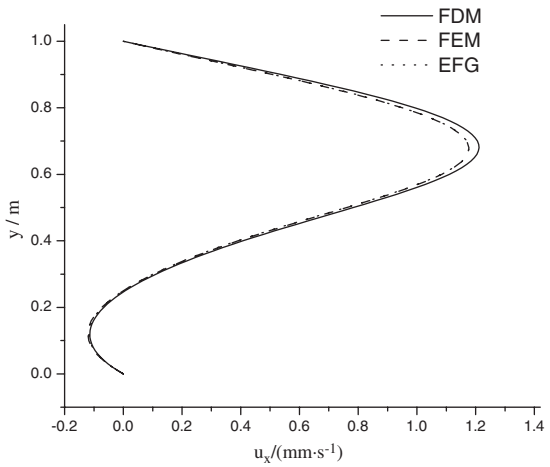

Figure 4. u_x distribution at $X = 2.5$ m for flow past a step.

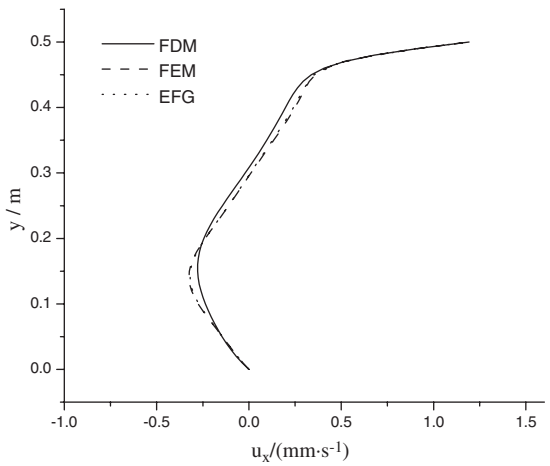

Figure 5. u_x distribution at $X = 2.5$ m for flow in a driven cavity.

DOI: 10.1002/fld

the computational domain are fixed in advance, the computational precision cannot be improved without changing the interpolating polynomial, unless new nodes are added into the domain, which will introduce programming related to the remeshing because of the replacing of the original mesh structure.

With the EFG method, although it is certainly necessary for adding new nodes to enhance the precision in a specific domain, there are cheaper methods that can be used in EFG to enhance the precision, such as increasing the number of background cells or enlarging the radius of the weight function supports will also improve the accuracy. Adding new nodes in FEM and FDM needs grid reconstruction. At the same time, if new nodes are added to the domain, there is no need to make any changes to the programs since no mesh structure connects the nodes with the meshless method. This flexibility is a substantial advantage of meshless methods in comparison with the FEM.

Moreover, when nodes in the computational domain are poorly distributed, the FEM probably distorts some elements that can affect the accuracy.

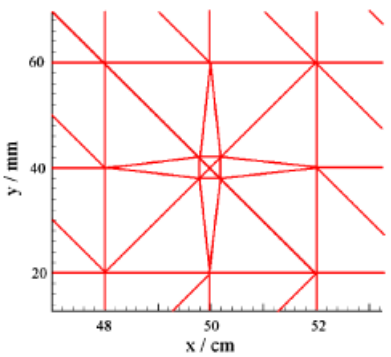

Figure 6. Distorted meshes generated by FEM.

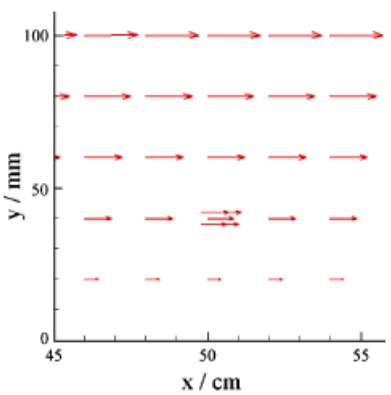

Figure 7. EFG results with poorly distributed nodes.

DOI: 10.1002/fld

As shown in Figure 6, distorted meshes occur when the nodes are not evenly distributed. With the FEM, non-uniform meshes require a smaller time step to ensure convergence, which greatly increases the computational expense.

When the EFG method encounters such a non-uniform mesh, the instability due to the poorly distributed nodes can be effectively eliminated by increasing the number of background cells and by enlarging the radius of the supports. With these remedies, a smaller time step is not needed, which will save computational time. With the four poorly distributed nodes in Figure 6, which are too close to the node in the center, the EFG results in Figure 7 show that the simulation is not adversely affected by this poor node distribution.

Furthermore, overlapping nodes can also be handled by the EFG method when the FEM would fail. As shown in Figure 8, where the position of two overlapping nodes is denoted by a black point at $x=50\,\text{cm}$, $y=40\,\text{mm}$, the EFG method still gives excellent results.

With verifying the effectiveness of the EFG method, flow around a cylinder was simulated for different Reynolds numbers. The computational domain is shown in Figure 9.

The calculations used $D=1\,\text{m}$, a fluid density $\rho=1.0\,\text{kg/m}^3$ and a parabolic velocity profile at the inlet:

$$\begin{aligned} u_x &= \frac{6U}{H^2}[(y-y_B)H-(y-y_B)^2] \\ u_y &= 0 \end{aligned} \tag{14}$$

where $U=1.0\,\text{m/s}$ is the mean velocity at the inlet; $H=4.1D$ is the height of the channel. The flow simulations used cylinder Reynolds numbers of 20, 100, 200 and 1000. The results are shown in Figure 10.

The results in Figure 10 show that for low Reynolds numbers ($Re=20, t=100\,\text{s}$), symmetric vortices form behind the cylinder. With increasing Reynolds number, the vortices behind the cylinder grow and become asymmetric. Above a critical Reynolds number (which for a cylinder in an infinite stream is about 40), the flow becomes unsteady and vortices are shed from the cylinder. The flow at $Re=100$ went through a development stage and eventually became periodic with a

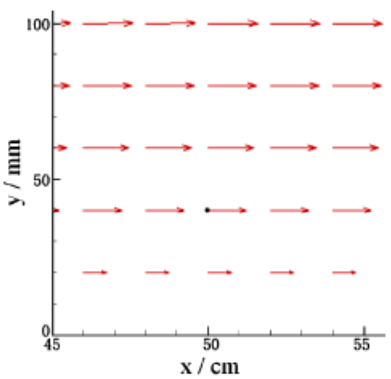

Figure 8. EFG results with overlapping nodes.

DOI: 10.1002/fld

Karman vortex street behind the cylinder. For $Re > 100$, more vortices occurred as shown in the figure. At $Re = 1000$, the numerical result was still stable although the convection effect was very strong.

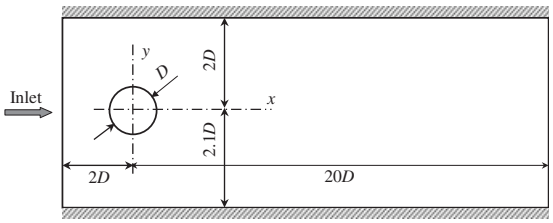

Figure 9. Computational domain for 2D, viscous, incompressible flow around a cylinder.

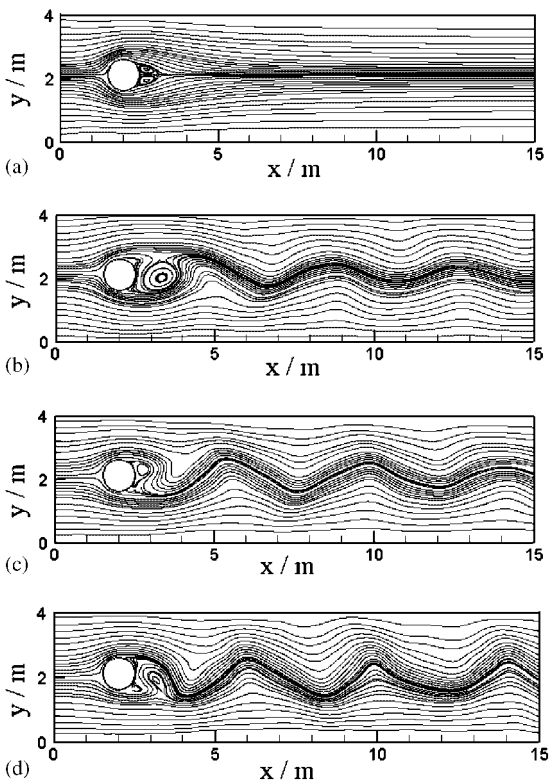

Figure 10. Streamlines around a cylinder for different Reynolds numbers: (a) $Re = 20, t = 100\,\text{s}$; (b) $Re = 100, t = 100\,\text{s}$; (c) $Re = 200, t = 100\,\text{s}$; and (d) $Re = 1000, t = 82\,\text{s}$.

DOI: 10.1002/fld

The vortex shedding causes both the drag and lift forces to oscillate. The drag and lift coefficients were defined as

$$C_{\mathrm{d}} = \frac{f_x}{\rho U^2/2}$$
$$C_{\mathrm{l}} = \frac{f_y}{\rho U^2/2} \tag{15}$$

where f_x and f_y are the x and y components of the force exerted by the fluid on the cylinder. These forces were calculated by integrating the pressure and shear forces over the cylinder surface.

Figure 11 shows the variation of the lift and drag coefficients on the cylinder in the channel at $Re = 100$ for the computational domain shown in Figure 9. If the domain were fully symmetric,

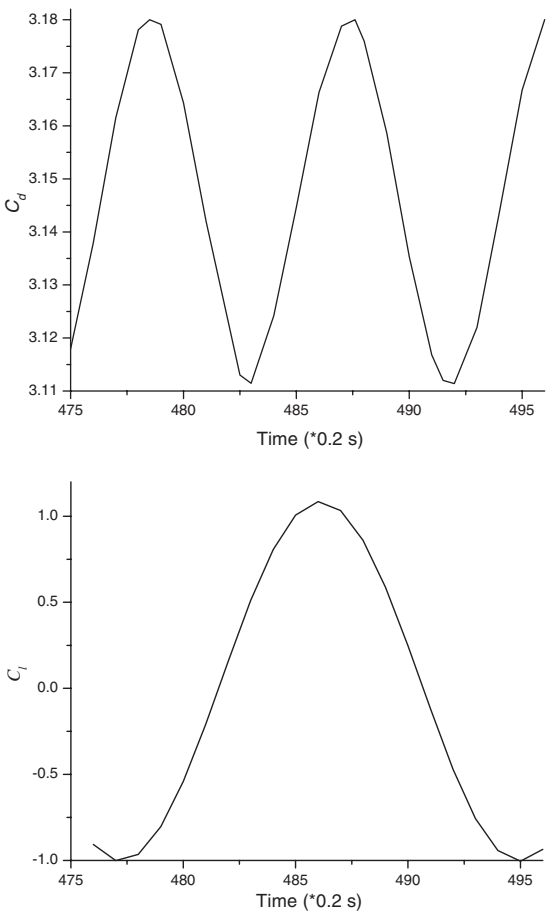

Figure 11. Drag (above) and lift (below) coefficients on a cylinder in a channel at $Re = 100$.

DOI: 10.1002/fld

the lift coefficient would oscillate around zero. However, the lift coefficient for the unsymmetrical flow oscillates between $C_{\mathrm{l,min}} = -1.004$ and $C_{\mathrm{l,max}} = 1.085$. The drag coefficient oscillates between $C_{\mathrm{d,min}} = 3.111$ and $C_{\mathrm{d,max}} = 3.180$.

Figure 11 shows that the drag force oscillates at twice the frequency of the lift force. The drag force has one maximum and one minimum during the growth and shedding of each vortex first from the top and then from the bottom of the cylinder, while the sign of the lift force depends on the vortex location, i.e. whether it is above or below the cylinder. The Strouhal number is defined as

$$S_t = \frac{D}{UT} \tag{16}$$

where T is the oscillation period for C_{l}. For these calculations, T was about 3.4 s at $Re = 100$ with the corresponding Strouhal number of 0.294 which is very close to 0.3018 given by Joel and

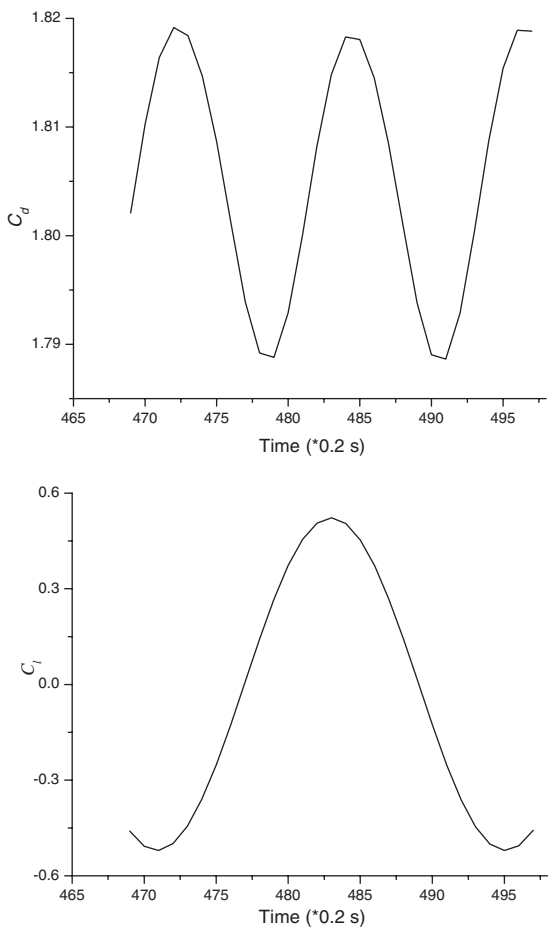

Figure 12. Drag (above) and lift (below) on a cylinder in an unconfined channel.

DOI: 10.1002/fld

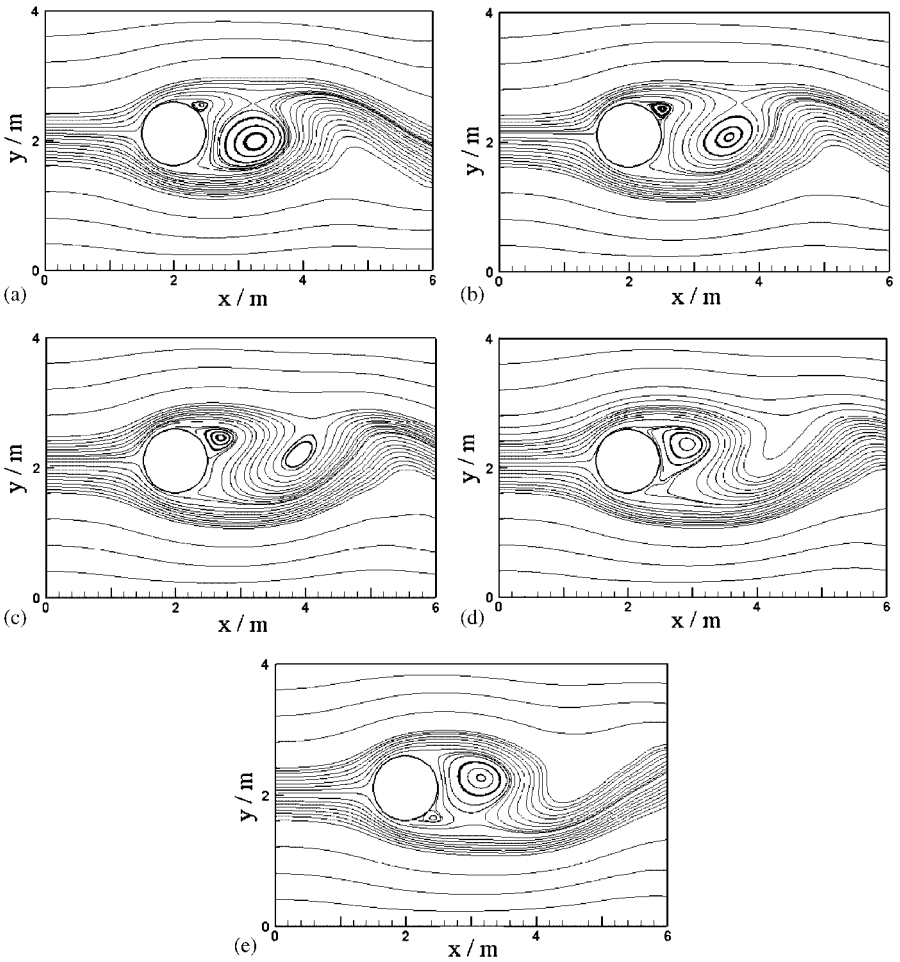

Figure 13. Variation of streamlines around a cylinder at $Re=100$ for half a period: (a) $t=78.2$ s; (b) $t=78.6$ s; (c) $t=79.0$ s; (d) $t=79.4$ s; and (e) $t=79.8$ s.

Milovan [14]. The confinement by the channel accelerates the vortex shedding; hence, the Strouhal number is much higher than for a cylinder in an infinite steam. An unconfined flow around a cylinder was also simulated with the Strouhal number being 0.204 for the lift coefficient data in Figure 12 (the standard value is 0.18–0.2 [14]).

The vortex shedding process was investigated in more detail for $Re=100$. Figure 13 shows the variation of the streamlines around a cylinder for one cycle. At $t=78.2$ s, a small vortex forms near the top of the cylinder. The vortex then expands and moves forward of the centerline of the cylinder. At $t=79.8$ s, another small vortex forms near the bottom of the cylinder. This completes one half of the vortex shedding period with a corresponding Strouhal number of 0.3125, which is very close to that given by Joel and Milovan [14].

DOI: 10.1002/fld

5. CONCLUSIONS

A comparison of the EFG and FEM methods shows that the precision of the EFG is better than FEM with the same quantities of grid nodes. It is certainly necessary for adding new nodes to enhance the precision in specific domain. However, adding new nodes in FEM needs grid reconstruction. There are cheaper methods that can be used in EFG to enhance the precision, such as increasing the number of background cells or enlarging the radius of the weight function supports will also improve the accuracy. When new nodes are added, the FEM needs to partly or fully remesh, while the EFG method can continue to calculate. The EFG method more easily handles poorly distributed nodes or even overlapping nodes. Although consuming more time, the EFG method is very promising for a great many complex problems such as interface/free-face flows and multiphase flows because of the advantages.

The flow around a cylinder for different Reynolds numbers was also simulated with the EFG method. The results by the EFG method agree well with previous studies, which shows that EFG can effectively simulate laminar flow as an additional, very flexible computational method for complex fluid mechanics problems.

The restriction of meshes makes particle collision problem in multiphase flows very difficult for mesh-based direct numerical simulation methods to deal with cases where there are particle collisions. Hence, the particle collision is a key problem in the direct numerical simulation of in multiphase flows. The research in this paper shows that it is possible and precise to simulate the fluid dynamics problems, laying the foundation for realizing real collisions between particles with the EFG method. This will be done in our further research.

ACKNOWLEDGEMENTS

The research was supported by the National Natural Science Foundation of China (No. 50432040) and the Special Funds for Major State Basic Research Projects (No. 2006CB200305).

REFERENCES

1. Lucy LB. A numerical approach to the testing of the fission hypothesis. *Astronomical Journal* 1977; **8**:1013–1024.
2. Liu WK, Jun S, Zhang YF. Reproducing kernel particle methods. *International Journal for Numerical Methods in Engineering* 1995; **20**:1081–1106.
3. Nayroles B, Touzot G, Villon P. Generalizing the finite element method: diffuse approximation and diffuse elements. *Computational Mechanics* 1992; **10**:307–318.
4. Belytschko T, Gu L, Liu YY. Fracture and crack growth by element-free Galerkin methods. *Modelling and Simulation in Materials Science and Engineering* 1994; **2**:519–534.
5. Song K, Lu M, Zhang X. Meshless method for solid mechanics. *Advances in Mechanics* 2000; **30**:55–65.
6. Liu Q, Shui H, Zhang X. Advances in numerical simulation of interfacial/free-surface flows. *Advances in Mechanics* 2002; **32**(2):259–274.
7. Belytschko T, Krongauz Y, Organ D, Fleming M, Krysl P. Meshless methods: an overview and recent developments. *Computer Methods in Applied Mechanics and Engineering* 1996; **139**:3–47.
8. Joseph DD. Interrogations of Direct Numerical Simulation of Solid–Liquid Flows, 2002 (Available from: http://www.efluids.com/efluids/books/joseph.htm).
9. Lancaster P, Salkauskas K. Surfaces generated by moving least-squares methods. *Mathematics of Computation* 1981; **37**:141–158.
10. Luo S, Cai Y, Zhang X. Object-oriented element free Galerkin method. *Chinese Journal of Mechanical Engineering* 2000; **36**(10):23–26.

DOI: 10.1002/fld

11. Jiang C, Xu Z, Li X. Fractional step finite element formulation for solving incompressible flows. *Journal of Tsinghua University* (*Science and Technology*) 2002; **42**(2):278–280.
12. Belytschko T, Lu YY, Gu L. Element free Galerkin method. *International Journal for Numerical Methods in Engineering* 1994; **37**:229–256.
13. Liu GR, Gu Y. *An Introduction to Meshfree Methods and their Programming*. Springer: Berlin, 2005; 110–150.
14. Joel HF, Milovan P. *Computational Methods for Fluid Dynamics*. Springer: Germany, 2002.

DOI: 10.1002/fld